



## Bifurcation and sensitivity analysis reveal key drivers of multistability in a model of macrophage polarization



Anna S Frank<sup>a</sup>, Kamila Larripa<sup>b</sup>, Hwayeon Ryu<sup>c</sup>, Ryan G. Snodgrass<sup>d</sup>, Susanna Röblitz<sup>a,\*</sup>

<sup>a</sup> Computational Biology Unit, Department of Informatics, University of Bergen, Bergen, Norway

<sup>b</sup> Department of Mathematics, Humboldt State University, Arcata, CA, USA

<sup>c</sup> Department of Mathematics and Statistics, Elon University, Elon, NC, USA

<sup>d</sup> Institute of Biochemistry, Goethe-University, Frankfurt, Germany

### ARTICLE INFO

#### Article history:

Received 2 July 2020

Revised 24 September 2020

Accepted 1 October 2020

Available online 9 October 2020

#### Keywords:

Dynamical Systems

Steady States

Cellular Signaling

Phenotypes

### ABSTRACT

In this paper, we present and analyze a mathematical model for polarization of a single macrophage which, despite its simplicity, exhibits complex dynamics in terms of multistability. In particular, we demonstrate that an asymmetry in the regulatory mechanisms and parameter values is important for observing multiple phenotypes. Bifurcation and sensitivity analyses show that external signaling cues are necessary for macrophage commitment and emergence to a phenotype, but that the intrinsic macrophage pathways are equally important. Based on our numerical results, we formulate hypotheses that could be further investigated by laboratory experiments to deepen our understanding of macrophage polarization.

© 2020 The Author(s). Published by Elsevier Ltd. This is an open access article under the CC BY license (<http://creativecommons.org/licenses/by/4.0/>).

### 1. Introduction

Monocytes are immune cells that circulate in the blood and are recruited to (cancer) tissue (Orekhov et al., 2019), where they differentiate into macrophages. Macrophages are highly versatile immune cells which, among other roles, eliminate pathogens and damaged cells through phagocytosis. They play a critical role in innate immunity and help to initiate the adaptive immune response through antigen presentation and cytokine signaling. Due to their diverse functions and plasticity, macrophages are able to exhibit markedly different phenotypes, depending on the external signals they receive, e.g., microbial products, damaged cells, or cytokines. For example, based on cytokines stimulation, macrophages will polarize into different phenotypes, which can be activated (e.g., M1 or M2) or non-activated (e.g., M0) (Orekhov et al., 2019). The continuum of macrophage activation and the diverse spectrum of pro- and anti-inflammatory phenotypes result in nuanced immune regulations (Mosser and Edwards, 2008).

A conceptual framework has been developed for the description of macrophage activation with two polar extremes being the most widely studied and best understood. On one end of the phenotype spectrum, M1-like macrophages are classically activated by the

cytokine interferon  $\gamma$  (IFN $\gamma$ ) or by an endotoxin directly (Medzhitov, 2008). Once activated, M1-like macrophages release cytokines that inhibit the proliferation of nearby cells (including cancer cells) and initiate inflammation and an immune response.

At the other extreme, M2-like macrophages are induced by the interleukins (IL)-4 and -13, cytokines secreted by activated Th2 cells (Gordon, 2003). They tend to dampen inflammation and promote tissue remodeling and tumor progression, for example through pro-angiogenic properties (Brown et al., 2017), immunosuppression (e.g., IL-10 expression) (Kuang et al., 2009), remodeling of the extracellular matrix, or promotion of metastasis (Lin et al., 2001).

Mixed phenotypes also exist, which share some (but not all) significant features with the M1- or M2-like phenotypes (Biswas and Mantovani, 2010). The existence of mixed phenotypes has been particularly demonstrated in the tumor microenvironment (Umemura et al., 2008).

Macrophage polarization is mediated in part, through the canonical Janus- or TYK2-kinases (JAK)-Signaling signal transducers and activators of transcription (STAT) signaling pathway. Activation of STATs is primarily driven by ligand-stimulated cytokine receptors whereby STATs become phosphorylated at a critical tyrosine residue leading to their release from the receptor complex where they then cross the nuclear membrane and reach chromatin. There they bind specific cognate DNA elements and participate in complex gene regulation processes. STAT phosphorylation kinetics have been extensively investigated in myeloid cells including

\* Corresponding author.

E-mail addresses: [Anna-Simone.Frank@uib.no](mailto:Anna-Simone.Frank@uib.no) (A.S. Frank), [kamila.larripa@humboldt.edu](mailto:kamila.larripa@humboldt.edu) (K. Larripa), [hryu@elon.edu](mailto:hryu@elon.edu) (H. Ryu), [snodgrass@biochem.uni-frankfurt.de](mailto:snodgrass@biochem.uni-frankfurt.de) (R.G. Snodgrass), [Susanna.Roblitz@uib.no](mailto:Susanna.Roblitz@uib.no) (S. Röblitz).

macrophages. Following stimulation with cytokine signals, STAT phosphorylation, nuclear localization and DNA binding occur (Dickensheets et al., 1999; Namgaladze et al., 2015; Goenka and Kaplan, 2011; Kovarik et al., 1999). The balance between activation of STAT1 and STAT6 tightly regulates macrophage polarization and activity (Wang et al., 2014).

Therefore, the phenotype expressed by a macrophage is identified through the specific STAT activation. M1 polarization is associated with STAT1 activity, whereas M2 polarization is associated with STAT6 activity (Martinez and Gordon, 2014).

The M1 and M2 polarization process is dynamic and can be reversed under certain conditions. Individual macrophages can change their phenotype in response to local signaling cues (Wang et al. (2014); Lawrence and Natoli (2011); Zheng et al. (2017)). This can be especially pronounced in the tumor microenvironment and manifests in tumor associated macrophages, which can demonstrate both pro-tumoral and anti-tumoral activities (Saccani et al., 2006).

Therefore, a better understanding of the polarization process of macrophages has the potential to guide the development of targeted cancer therapy to redirect the polarization towards a tumor suppressing microenvironment (Williams et al. 2016; Zheng et al. 2017; Cheng et al. 2019).

Mathematical modeling is a useful tool to better understand macrophage polarization by validating or testing hypothesis, and making predictions about possible dynamics. To our knowledge, three previous studies based on ordinary differential equations (ODEs) have modeled macrophage polarization and plasticity (Smith et al. 2016; Nickaeen et al. 2019; Zhao et al. 2019). While the authors in Nickaeen et al. (2019) showed bistable dynamics of macrophage phenotypes when exposed to external signaling cues, the authors in Smith et al. (2016) could show that after initial differentiation into M1 and M2, the M2 phenotype was ultimately dominating. Finally, the authors in Zhao et al. (2019) used a systems-level approach to present the complexity of signaling pathways and intracellular regulation which describe macrophage differentiation under IFN- $\gamma$ , IL-4 signaling, and cell stress (hypoxia). With their model, the authors in Zhao et al. (2019) could replicate experimental results on macrophage phenotype markers and transcription factor regulations upon external perturbations, also for the tumor microenvironment.

All three models are built using generic formulations of self-stimulation and mutual inhibition, which are also common building blocks in immune cell differentiation models (Callard 2007; Yates et al. 2004). Similar modelling approaches as for T-cell differentiation have been used for macrophages in e.g., Nickaeen et al. (2019); Smith et al. (2016), as T-helper cells differentiate in a similar manner (Luckheeram et al. 2012; Martinez and Gordon 2014).

Our goal is to use mathematical modeling to shed light on the polarization and regulatory signaling dynamics related to activation of macrophage phenotypes by specifically tracking STAT1 and STAT6 activation levels as proxies for M1 and M2 polarization, respectively. We aim to build a simple model, which includes less parameters than the previous models, but which shows similar complex dynamics. We aim for simplification in model formulation both biologically and mathematically. For the biological aspect, we aim at a simplified circuitry, as opposed to other ODE models that consider more pathways, e.g. Smith et al. (2016, 2019), or that consider impact from other cells signaling in the immune system and cancer cells (Morales and Soto-Ortiz, 2018). We have consolidated a number of pathways in our model and are viewing macrophages in isolation other than an input signal. From a mathematical point of view, we present a 2-dimensional ODE model that is mathematically simpler than other non-ODE models with more complexity in their formulation, such as an agent-based approach (Nickaeen et al., 2019).

The relatively low dimension of our ODE model allows us to conduct bifurcation and stability analyses to study its dynamical diversity, and to relate these dynamics to biological observations. In addition, Sobol's method is employed to i) guide the model reduction and ii) to identify the most sensitive drivers of the system dynamics. Finally, sensitive parameters are altered to study their effect on the dynamics.

For the rest of this paper, Section 2 describes our mathematical model in context of macrophage polarization and Section 3 contains the conduction of the numerical methods. In Section 4, our main results, consisting of bifurcation analysis (Section 4.1), GSA (Section 4.2) and and perturbation analysis based on GSA results (Section 4.3), are presented. We conclude with the Discussion in Section 5. The Appendix section provides more details on numerical analysis and the applied methodology.

## 2. Mathematical model

Our mathematical model is based on the interactions specific to the macrophage lineage commitment signaling network. For this purpose, we simplify the network of macrophage functions in the liver from Sica et al. (2014), and consider only IFN $\gamma$  (input signal  $S_1$ ) and IL-4 (input signal  $S_2$ ) as relevant cytokine signals. The levels of activated STAT1 (variable  $x_1$ ) and STAT6 (variable  $x_2$ ) are used in our model as proxies for the two macrophage activation states.

A schematic diagram of our model is given in Fig. 1. We model the dynamics of activated STATs with a pair of coupled nonlinear differential equations, described in Eqs. (1,2). The Eqs. (1,2) were adapted from the T-cell model in Yates et al. (2004). They are similar, but not the same, since the equation for  $x_2$  has a different structure.

$$\frac{d}{dt}x_1 = (a_1 \cdot H^+(x_1, k_1, n_1) + S_1) \cdot H^-(x_2, p_2, l_2) + b_1 - q_1x_1, \quad (1)$$

$$\frac{d}{dt}x_2 = a_2 \cdot H^+(x_2, k_2, n_2) + S_2 \cdot H^-(x_1, p_1, l_1) + b_2 - q_2x_2, \quad (2)$$

$$H^+(x_i, k_i, n_i) = \frac{x_i^{n_i}}{x_i^{n_i} + k_i^{n_i}} \quad (3)$$

$$H^-(x_i, p_i, l_i) = \frac{p_i^{l_i}}{p_i^{l_i} + x_i^{l_i}}. \quad (4)$$

All parameters are assumed to be constant, positive and real numbers, except  $n_{1,2}$  and  $l_{1,2}$ , which are integers.

The description of all model parameters is provided in Table 1.

### 2.1. Model formulation

The equation for  $x_2$  is based on the assumption that both type I and type II interferons inhibit IL-4-induced STAT6 activation in

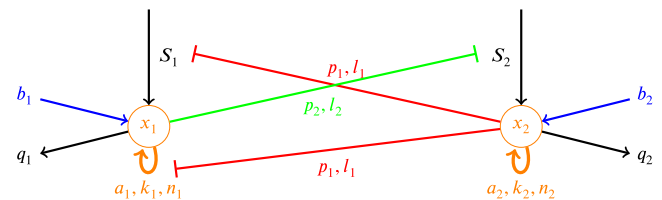


Fig. 1. Schematic Diagram of Mathematical Model in Eqs. 1,2. Self-stimulation of  $x_1$  and  $x_2$  are represented via the orange arrows, while processes of mutual-inhibition are shown by red and green inhibiting arrows. The incoming blue arrows depict  $x_1, x_2$  activation at basal rates (also in the absence of cytokine signaling), while the incoming black arrows represent the respective activation of  $x_1$  and  $x_2$  via cytokines ( $S_i$ ). Deactivation of  $x_{1,2}$  is illustrated by the outgoing black arrows. Note the asymmetry in that  $x_2$  (STAT2) inhibits both the input signal and self-stimulation, but  $x_1$  (STAT1) affects only the input signal.

**Table 1**

Model parameters in Eqs. 1, 2. Physical units for non-dimensionless parameters are given in parentheses.

Parameter	Description
$a_{1,2}$	Strength of self-stimulation (1/day)
$b_{1,2}$	Basal activation rates (1/day)
$n_{1,2}$	Exponents in the Hill functions for self-stimulation
$k_{1,2}$	Thresholds in the Hill functions for self-stimulation
$l_{1,2}$	Exponents in the Hill functions for mutual inhibition
$p_{1,2}$	Thresholds in the Hill function for mutual inhibition
$q_{1,2}$	Deactivation rates (1/day)
$S_{1,2}$	Input signal strength (1/day)

human monocytes in a SOCS-1-dependent manner (Dickensheets et al., 1999), and therefore differs from the model formulation in Yates et al. (2004). This change results in an asymmetry in our equations in that STAT6 inhibits both the input signal and self-stimulation, but STAT1 affects only the input signal (Venkataraman et al., 1999). Furthermore, we reduced model complexity by fixing the Hill coefficient in Eq. (4) to 1. Also, the signal input function in Yates et al. (2004) was simplified to a single parameter ( $S_1, S_2$ , respectively) for each phenotype in our model.

In our model equations, the parameters  $a_i$  represent the maximal activation rate of STAT due to self-stimulation. STATs are, however, also activated at low background levels ( $b_i$ ) in the absence of cytokine stimulation (Dempoya et al., 2012). STATs are also inactivated by dephosphorylation, and we assume this rate is linear (terms  $q_i x_i$  in the equations).

The fact that STAT1 and STAT6 are autocrine (Yarilina et al., 2008; Goenka and Kaplan, 2011), is captured by the stimulating Hill functions in the model Eqs. (1,2). Finally, we assume respective activation of STAT1 and STAT6 via  $IFN\gamma$  ( $S_1$ ) and IL-4 ( $S_2$ ) (Ohmori and Hamilton, 1997).

We use stimulating (Eq. (3)) and inhibiting (Eq. (4)) Hill functions to describe STAT self-stimulation and mutual inhibition (Tyson and Novák, 2010), respectively. The rationale behind the choice of these generic functions is that self-stimulation and inhibition are complex, non-linear processes, which consist of several individual steps. For example, in the process of self-stimulation, cytokines from the macrophage are secreted to stimulate helper T-cell differentiation (Lee, 2019). Differentiated helper T-cells then secrete cytokines which in-turn stimulate the macrophage differentiation. However, detailed knowledge about these individual steps is unknown, which makes it difficult to derive mathematical equations for each step. In addition, we assume that the response in self-stimulation is sigmoidal, depending on the “dose” of input signals. Therefore, the Hill function is used and replaces the need to model the steps individually (Tyson and Novák, 2010). A similar argument was used for the inhibitory Hill function.

In the Hill function of Eq. (3),  $k_i$  represents the signaling level at which STAT stimulation is half-maximal and the Hill coefficient  $n_i$  governs the steepness of the Hill function in that as this value grows, the function becomes more switch-like. For the inhibitory Hill function, the parameters play a similar role.

### 3. Numerical methods

In this section we provide a detailed description of the numerical methods we employed.

#### 3.1. Selection of model parameters

We explore parameter variations and analyze how the different parameter sets affect variability in the system states by using three parameter sets: the initial set  $\Theta_0$ , and two variation sets,  $\Theta_1$  and  $\Theta_2$ . The parameters in the initial set  $\Theta_0$  are adapted from Yates

et al. (2004), while the variation sets  $\Theta_1$  and  $\Theta_2$  are derived using nullclines.

Parameter sets  $\Theta_0$  and  $\Theta_1$  are justified, because (i) the model formulation is very similar to the one in Yates et al. (2004), (ii) macrophage and T-cell immune responses are connected with respect to, e.g., cytokine signaling (Lee, 2019), and (iii) both immune response processes occur in the cell micro-environment. Given the preceding arguments, the same parameter units as in Yates et al. (2004) apply here. Since parameter set  $\Theta_2$  was derived from  $\Theta_0$  and  $\Theta_1$  by exploring the numerical properties of the macrophage model, we consider this parameter set also as biologically valid. All three parameter cases are presented in Table 2.

The only difference between  $\Theta_0$  and  $\Theta_1$ , is the input signal values representing cytokine signal concentrations ( $S_i = 3.75$  vs.  $S_i = 4$  for  $i = 1, 2$ ). The increase in  $S_i$  values from  $\Theta_0$  to  $\Theta_1$  could resemble a change in environmental conditions, in which input signal strength increases. Also, this change is made based on the nullclines using  $\Theta_0$  so that the set  $\Theta_1$  results in qualitatively different model dynamics.

Given the model results from  $\Theta_1$ , we further make parameter variations for  $\Theta_2$ . Specifically, we increase the strength of self-stimulation,  $a_i$ , and degradation rate  $q_i$  for each variable. The last change is in the parameter  $n_1$  that has been substantially increased to incorporate the enhanced self-stimulating effect for  $x_1$ .

Finally, recall that the Hill exponents  $l_i$  are set to 1 for all three parameter sets considered. This choice is based on global sensitivity analysis, in which those coefficients are not shown as sensitive parameters to the model dynamics. Moreover, due to the asymmetry in the model equations, an exponent of one in the Hill functions representing mutual inhibition is sufficient to cause multistability, in contrast to, e.g., the Collins toggle switch model (Gardner et al., 2000), which requires Hill exponents larger than one for bistability.

#### 3.2. Bifurcation and stability analysis

We expect our model, for all three case scenarios,  $\Theta_{0,1,2}$ , to exhibit at least bistable dynamics, similar to the original model. Thus, we first conduct bifurcation analysis to further investigate the impact of different parameter sets on model dynamics.

Bifurcation analysis aims to detect critical points of the bifurcation parameters, where the system dynamics change qualitatively in the long-term (Gul et al., 2018). Given the biological importance of external signaling cues ( $IFN\gamma$  and IL-4) in the macrophage polarization process (Wang et al., 2014), we are primarily interested in determining how the system dynamics change based on varying input signals (i.e.,  $S_1$  and  $S_2$ ). We therefore consider  $S_1$  and  $S_2$  as main bifurcation parameters, with the other parameters set to their values in Table 2. The bifurcation diagrams from Eqs. (1,2) were obtained using the software package XPPAUT (Ermentrout, 2001). Details on numerical settings to draw bifurcation diagrams can be found in Appendix A.1.

We define states of STAT activation based on model-specific thresholds. An activation level is defined as *low*, if  $x_{1,2} \leq 1.0$ , and as *high*, if  $x_{1,2} > 1.0$ . It is then the ratio of STAT1 to STAT6 activation, that characterizes a macrophage phenotype. The threshold levels are chosen to allow a consistent classification of phenotype cases in our model, although they only represent relative levels.

Stability analysis was performed by numerical simulations in Matlab.

#### 3.3. Sensitivity analysis

We perform sensitivity analysis to identify parameter sets that have the greatest influence on the model outputs (e.g., STAT1 and STAT6 activation), and act as key drivers of macrophage polariza-

**Table 2**

Parameter sets for numerical scenarios. The initial set  $\Theta_0$  is adapted from Yates et al. (2004). In the two variation sets  $\Theta_{1,2}$ , bold numbers indicate the variations made compared to the initial set  $\Theta_0$ .

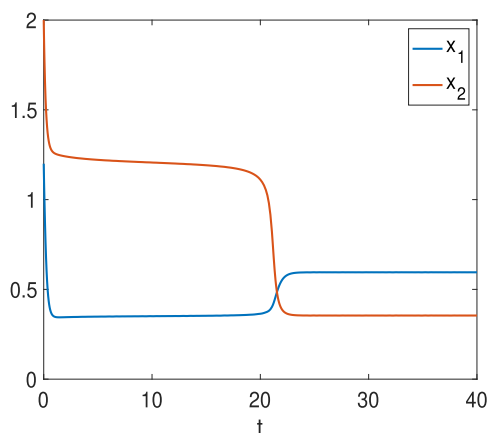
Set	$a_1$	$a_2$	$b_1$	$b_2$	$n_1$	$n_2$	$k_1$	$k_2$	$l_1$	$l_2$	$p_1$	$p_2$	$q_1$	$q_2$	$S_1$	$S_2$
$\Theta_0$	5	5	0.05	0.05	6	6	1	1	1	1	0.5	1	5	5	3.75	3.75
$\Theta_1$	5	5	0.05	0.05	6	6	1	1	1	1	0.5	1	5	5	<b>4</b>	<b>4</b>
$\Theta_2$	<b>15</b>	<b>8</b>	0.05	0.05	<b>22</b>	6	1	1	1	1	0.5	1	<b>5.8</b>	<b>5.8</b>	<b>5</b>	<b>5</b>

tion. Local sensitivity analysis quantifies changes in the model with respect to perturbation of a single parameter at-a-time in the parameter space (Zi, 2011). In contrast to local sensitivity, Global Sensitivity Analysis (GSA) methods explore the effects of large variations of parameter values on model outcome by varying all parameters simultaneously. This difference makes GSA methods more applicable in cellular environments, where it is possible that multiple input parameters vary simultaneously within a large parameter range. We chose Sobol’s method (Sobol, 2001) because it makes no assumptions about the relationship between model inputs and outputs in contrast to, for example, the Partial Rank Correlation Coefficient method, which requires monotonicity. Additionally, Sobol’s method considers interactions between parameters. A detailed description of Sobol’s method can be found in Appendix A.2.

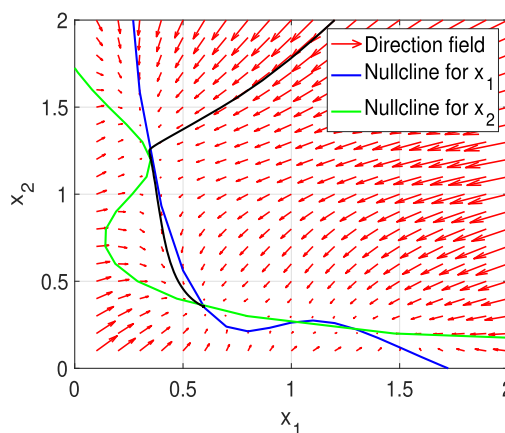
We implemented Sobol’s sensitivity analysis using the SALib package (Herman and Usher, 2017). We varied parameters 15% in each direction from their baseline values (i.e., parameter sets  $\Theta_{0,1,2}$  in Table 2). We consider these scenarios separately. In all cases, we generated 300,000 parameter set samples. The selected outcome of interest for the analysis is the ratio of STAT1 to STAT6 activation, which is responsible for macrophage polarization to specific phenotypes.

3.3.1. Perturbation in sensitive parameters

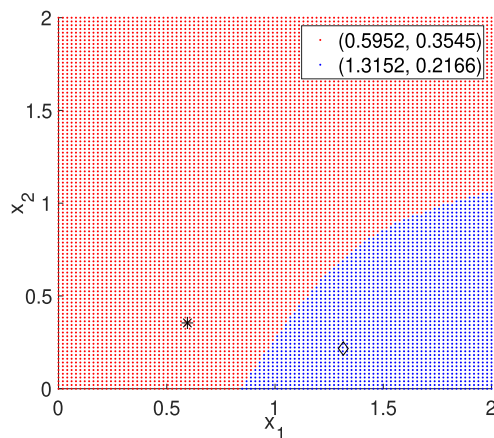
Based on results of the GSA, we explore the effect of perturbations in sensitive parameters on macrophage polarization dynamics. Firstly, to give an illustrative example, we will only consider perturbations in the most sensitive parameter ( $q_2$ ) on case  $\Theta_0$ . Understanding the effect of dephosphorylation on system dynam-



(a) Switch Behavior



(b) Phase Plane with Trajectory



(c) Basin of Attraction

**Fig. 2.** (a): Numerical solution that converges to low/low steady state after switch with initial condition  $(x_1, x_2) = (1.2, 2)$ ; (b): its corresponding trajectory (in solid black) in the phase plane; (c): the basin of attraction for both stable fixed points.

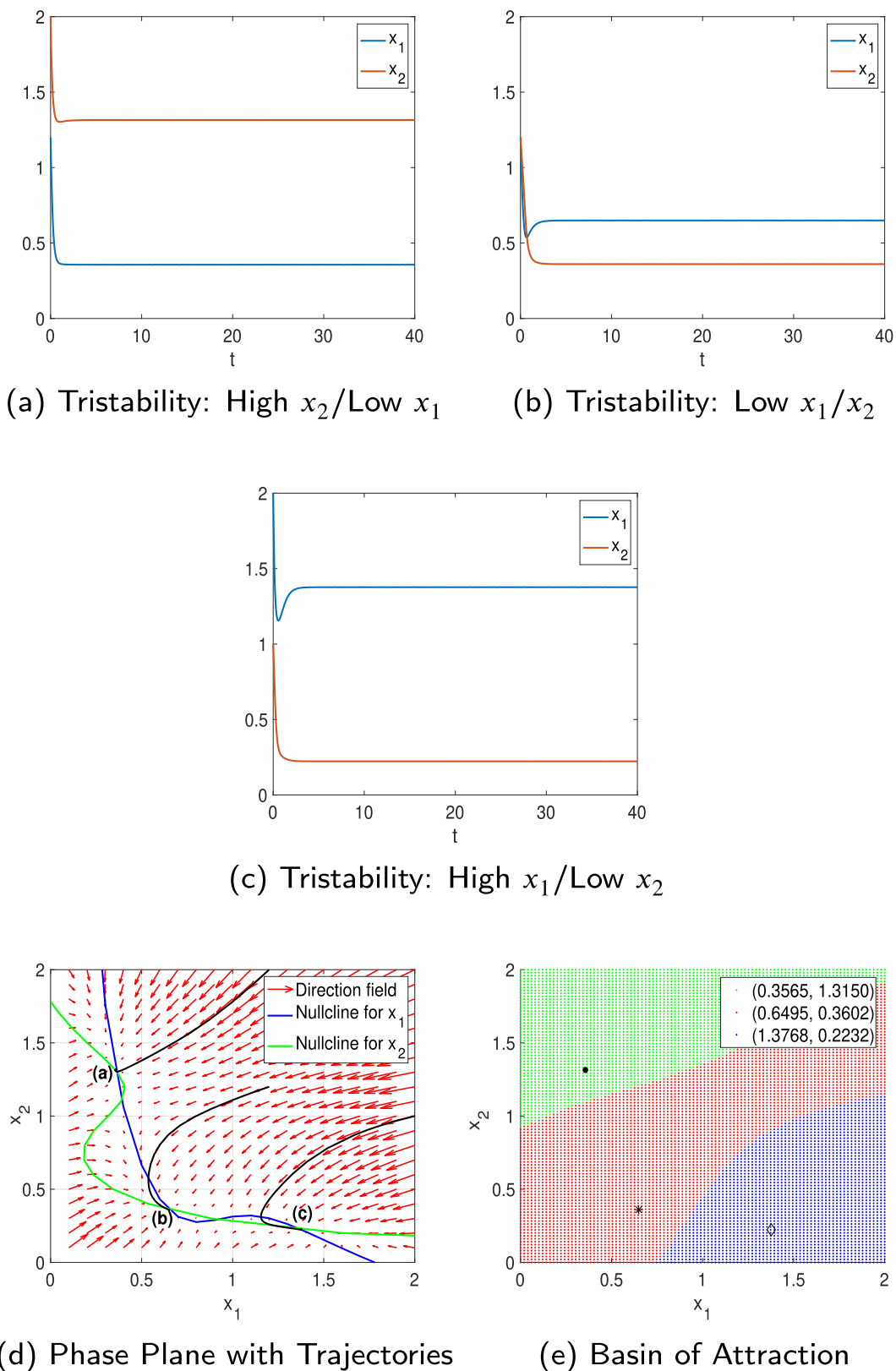


**Fig. 3.** (a)–(c): Numerical solutions that converge to three different stable steady states with initial conditions (a)  $(x_1, x_2) = (1.2, 2)$ , (b)  $(x_1, x_2) = (1.2, 1.2)$ , and (c)  $(x_1, x_2) = (2, 1)$ ; (d): their corresponding trajectories (in solid black) in the phase plane; (e): the basin of attraction for each stable fixed point.

ics is especially important as deactivation rates change often in biological settings (ten Hoeve et al., 2002). We change  $q_2$  and keep all other parameters fixed. This demonstrates the parameter’s indi-

vidual effect on the relation between external input signals and activation of transcription factors. Secondly, since there exists a biochemical difference in STAT1 de-/phosphorylation compared

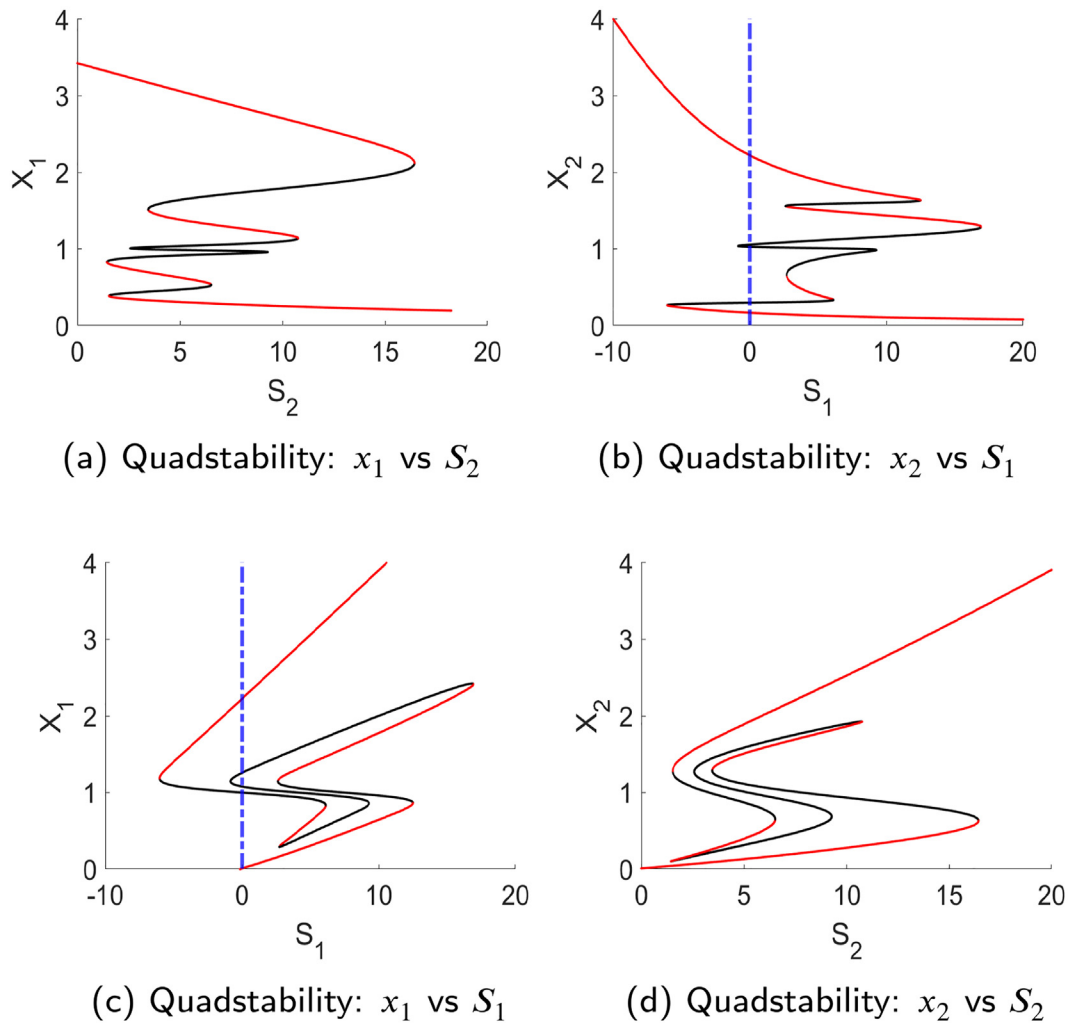


**Fig. 4.** The bifurcation diagrams for varying input signals ( $S_1$  and  $S_2$ ) against the state variables  $x_1$  and  $x_2$  show quadstable dynamics (with the set  $\Theta_2$ ). The red solid lines represent stable fixed points, while the black solid lines represent unstable fixed points and saddle-nodes. The blue dashed line represents the situation where  $S_1 = 0$ . (For interpretation of the references to colour in this figure legend, the reader is referred to the web version of this article.)

to STAT6 (Droescher et al., 2011.), we will model faster STAT1 deactivation rates ( $q_1$ ) and investigate their effect on model dynamics.

#### 4. Model results

The results of the numerical simulations are presented in this section.

##### 4.1. Bifurcation and stability analysis reveal multistable macrophage phenotypes

We observe bistability, tristability, and quadstability for different combinations of  $S_1$  and  $S_2$  based on the three parameter cases  $\Theta_{0,1,2}$ , respectively.

###### 4.1.1. Bistable case

With the initial parameter set  $\Theta_0$  we observe two stable fixed points, exhibiting bistable behavior. These steady states represent state variable ratios ( $x_1/x_2$ ) with i) high/low and ii) low/low levels.

Detailed bifurcation diagrams are presented in Fig. 8 in Appendix A.3. We validate this bistable behavior by numerically solving Eqs. (1,2) with the parameter set  $\Theta_0$ . The most interesting behavior observed is that  $x_1$  and  $x_2$  go through a switch before converging to

their respective stable fixed points, as shown in Fig. 2(a). The solution trajectory of this switch behavior (in solid black) in the phase plane is provided in Fig. 2(b). Note that only two fixed points are present even though there seems to be another fixed point on the upper left part in the phase plane because of the proximity of the  $x_1$ - and  $x_2$ -nullclines. The bistable behavior is further confirmed by the basin of attraction shown in Fig. 2(c).

###### 4.1.2. Tristable case

With parameter set  $\Theta_1$ , three stable steady states of ( $x_1/x_2$ ) are observed with i) high/low, ii) low/low, iii) low/high, levels. The third state represents a situation where STAT6 is presented at high levels, while STAT1 is present at low levels.

Numerical solutions that converge to different stable fixed points are shown in Fig. 3(a)–(c). The respective solution trajectories in the phase plane are shown in Fig. 3(d).

Because of the increased values  $S_1 = S_2 = 4$  for this case, there are two additional intersections between the  $x_1$  and  $x_2$ -nullclines compared to the bistable case, as can be seen in the phase plane of Fig. 3(d). This results in the addition of two fixed points, one of which is stable and the other is unstable. Thus, if we start with the same initial condition used in Fig. 2(a), the trajectory converges to the new stable fixed point with high  $x_2$ /low  $x_1$ , which was not observed in the bistable case. As further confirmed by the basin

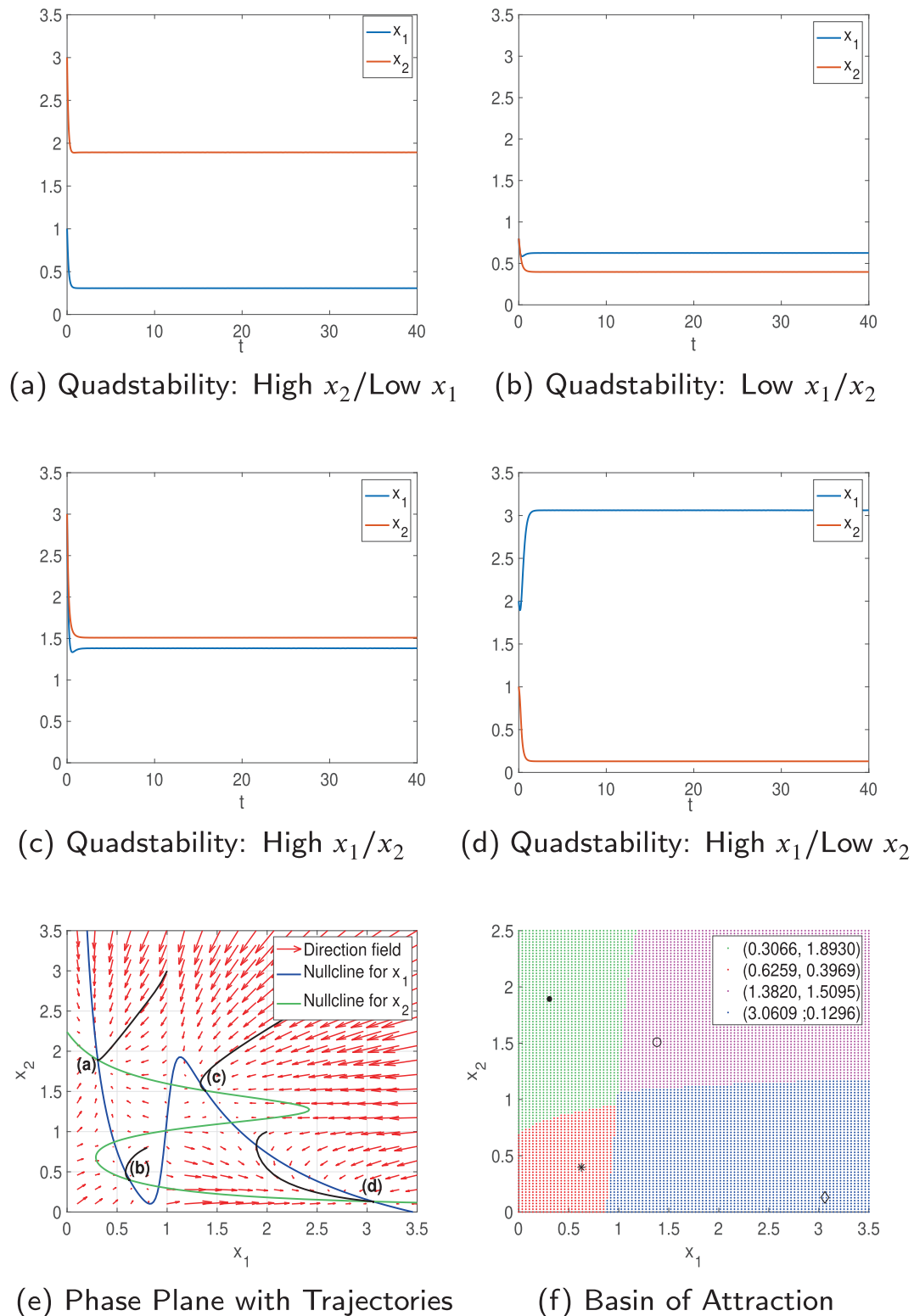


**Fig. 5.** (a)–(d): Numerical solutions that converges to four different stable steady states with initial conditions (a)  $(x_1, x_2) = (1, 3)$ , (b)  $(x_1, x_2) = (0.8, 0.8)$ , (c)  $(x_1, x_2) = (3, 3)$ , and (d)  $(x_1, x_2) = (2, 1)$ ; (e): their respective solution trajectories (in solid black) in the phase plane; (f): the basin of attraction for quadstable dynamics.

of attraction of Fig. 3(e), the other two stable fixed points remain as before. Bifurcation diagrams are presented in Fig. 9 in Appendix A.3.

It is the ratio of STAT1 ( $x_1$ ) to STAT6 ( $x_2$ ) activation levels that defines the polarization of a macrophage into the M1 or M2 phenotype (Wang et al., 2014; Nickaen et al., 2019). In our results, a high

level of activated STAT1 in presence of low activated STAT6 levels defines the M1 phenotype (Fraternal et al., 2015), while low levels of activated STAT1 and high levels of activated STAT6 define the M2 phenotype. Low STAT1 and STAT6 activation levels represent a “hyporesponsive” phenotype that has not been described in the current literature. This phenotype might however have biological

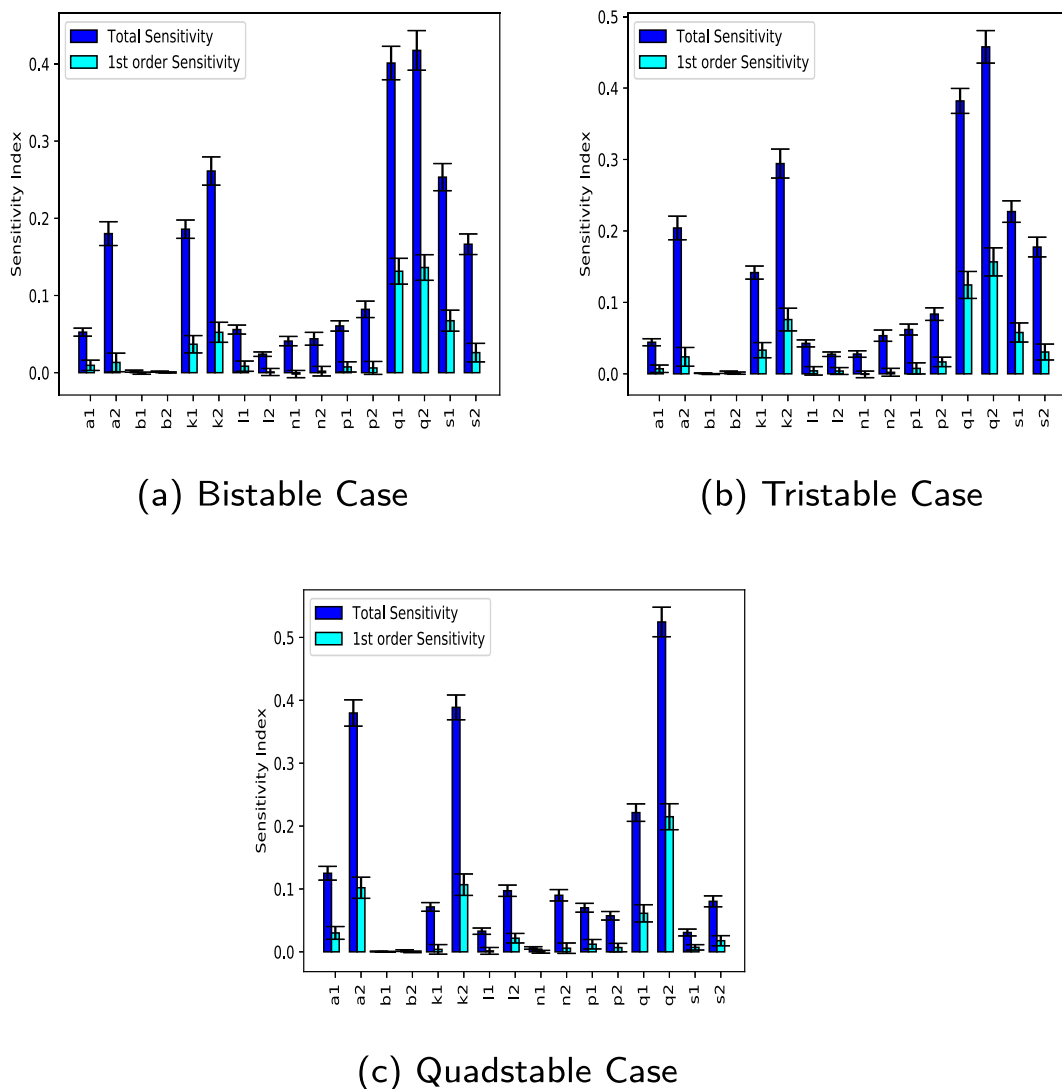


**Fig. 6.** Sobol Sensitivity Indices where outcome of interest is the ratio of STAT1 activation to STAT6 activation at steady state. This used baseline parameter values which give (a) bistable, (b) tristable and (c) quadstable dynamics. In all instances, the parameter  $q_2$  has the highest total sensitivity index. The cases of bistability and tristability have the same most sensitive seven parameters  $q_2, q_1, k_2, s_1, k_1, a_2, s_2$  with only the ordering of the last three altered. For the quadstable case,  $q_2$  is also the most sensitive, with  $k_2$  and  $a_2$  moving up in the ordering compared to the previous two cases.

relevance (e.g., for cancer therapy), as an intermittent phenotype between M1 and M2. For example, recent studies by Bronte and Murray (2015); Castiglione et al. (2016); Linde et al. (2012) have shown that tumors are initially characterized by M1 or an intermittent phenotype state, while advanced cancer is defined by M2 phenotype. It is therefore possible that this “hypo-responsive” phenotype describes another intermittent phenotype that appears during this transition.

#### 4.1.3. Quadstable case

Using the last parameter set  $\Theta_2$ , our model demonstrates quadstable behavior. The detailed bifurcation diagrams are provided in Fig. 4, where red solid lines represent stable fixed points, and black solid lines represent both unstable fixed points and saddle-nodes. Three of the stable fixed points, i.e., low/low, high/low and low/high, (in Fig. 4(a)–(d)) are qualitatively the same as those in the tristable case.

The situation where both STAT1 and STAT6 have high activation status is, however, unique to the quadstable case. High activation of both STAT1 and STAT6 shows the existence of an intermittent phenotype (Biswas and Mantovani, 2010), which bears characteris-

tics of both the M1 and M2 types. Several of such intermittent states have been identified, for example, M2a, M2b, M2c and M2d (Palma et al., 2018). The intermittent phenotype can also represent a transformation state, in which M1 branches to M2, and vice versa (Das et al., 2015).

To understand how a varying input signal changes the activation of STAT1 and STAT6, we illustrate, based on Fig. 4(b)–(c), how one should read the bifurcation diagram: Fig. 4(b)–(c) have to be read simultaneously, starting from  $S_1 = 0$  and then increasing the  $S_1$  value while following the bifurcation trend. Note that while  $S_1$  is varied, all other parameters values are kept unchanged. By varying  $S_1$  from 0 to around 12,  $x_1$  is on the lowest stable branch while  $x_2$  is on the highest stable branch. Increasing  $S_1$  input signal beyond 12,  $x_1$  and  $x_2$  will follow the bifurcation trend up and down, respectively, to the next stable branch with  $x_1$  activation level between 1 and 2.2, and  $x_2$  activation level between 1.8 and 1.3. To reach the third stable branch, input signal  $S_1$  is decreased (to follow the bifurcation trend) until  $x_1$  and  $x_2$  jump from the second red branch to the third branch. The third branch spans values between 0.3 and 1 for  $x_1$ , and values between 0.3 and 0.7 for  $x_2$ . When on the third branch,  $S_1$  input signal will be increased again,



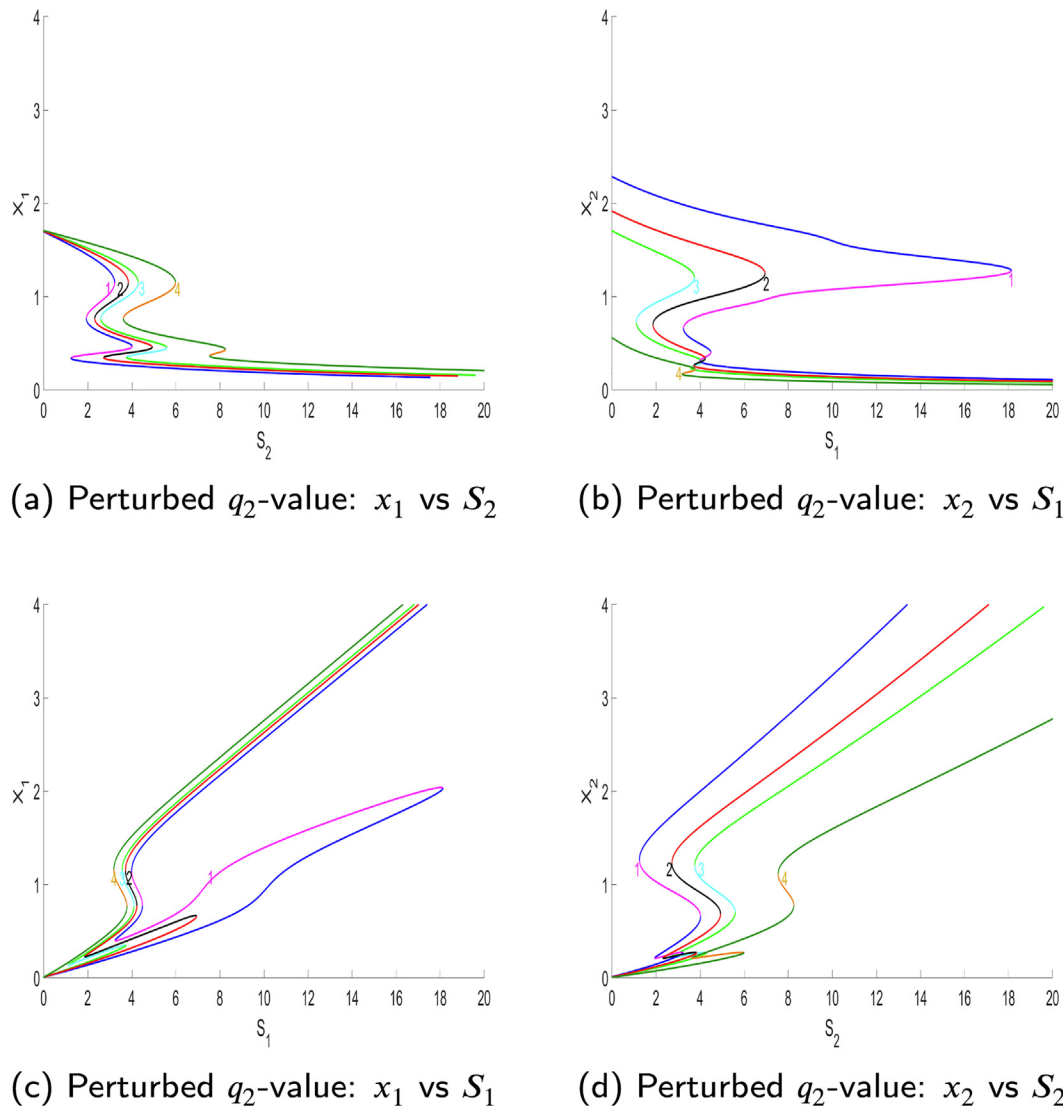


**Fig. 7.** Case  $\Theta_0$  for varying  $q_2$ -values ( $q_2 = 3.8$ -label 1,  $q_2 = 4.5$ -label 2,  $q_2 = 6.9$ -label 4) with respect to baseline  $q_2$ -value ( $q_2 = 5$ -label 3). The colors, magenta, black, turkeys and orange represent unstable branches, while blue, red, light green and dark green represent stable ones. (For interpretation of the references to colour in this figure legend, the reader is referred to the web version of this article.)

at an input signal of around 7, both  $x_1$  and  $x_2$  will jump onto the respectively highest and lowest branch. Fig. 4(a)–(d) can be read similarly.

In Fig. 4(b)–(c), we observe furthermore that for high,  $S_1 > 18$  levels, the state variables  $x_1$  and  $x_2$  are committed to highest and lowest activation levels, respectively.

It is interesting that in the case of quadstability, the system is committed to the high/low state (see Fig. 4(b)–(c)) for high  $S_1$  values, while this could not be observed for bistable or tristable situations. Biologically, an irreversible switch into the M1 phenotype means that the macrophage will no longer be able to change its phenotype when exposed to changing input signals. This suggests that for high self-stimulation in the presence of high  $INF\gamma$  and low IL-4 signals, the system can commit to M1 phenotype and stay reversible for the M2 phenotype. In parameter set  $\Theta_2$ , STAT1 has higher self-stimulation than STAT6, i.e.,  $a_1 > a_2$  and  $n_1 > n_2$ . This might be a crucial driver for the commitment in the quadstable case, and the emergence of the intermittent phenotype.

Numerical solutions that converge to different stable points are shown in Fig. 5(a)–(d). Their respective solution trajectories are presented in Fig. 5(e). The basin of attraction of Fig. 5(f) shows

the total of four stable fixed points, which indicates the quadstable dynamics.

#### 4.2. Identification of key drivers of macrophage dynamics through global sensitivity analysis

We applied Sobol’s method to the model output to identify the most sensitive parameters in our system. Because our goal is to identify phenotype commitment, and because we use STAT1 and STAT6 as proxies for the M1 and M2 phenotype, respectively, our model outcome of interest is the ratio of STAT1 and STAT6 at steady state:  $f(x) = \frac{x_1}{x_2}$  when  $dx_1/dt = dx_2/dt = 0$ . Details of the implementation are included in Appendix A.2. The most sensitive parameters for the bistable case using total sensitivity as a metric are, in descending order,  $q_2, q_1, k_2, S_1, k_1, a_2, S_2$  (see Fig. 6(a)). The four most sensitive parameters for bistable and tristable cases, shown in Fig. 6(a)–(b), respectively, agree and the next three most sensitive for each case are common ( $k_1, a_2, S_2$ ) but reordered. Fig. 6 (c) shows that the most sensitive parameters in the quadstable case are consistent with results from the previous two cases.

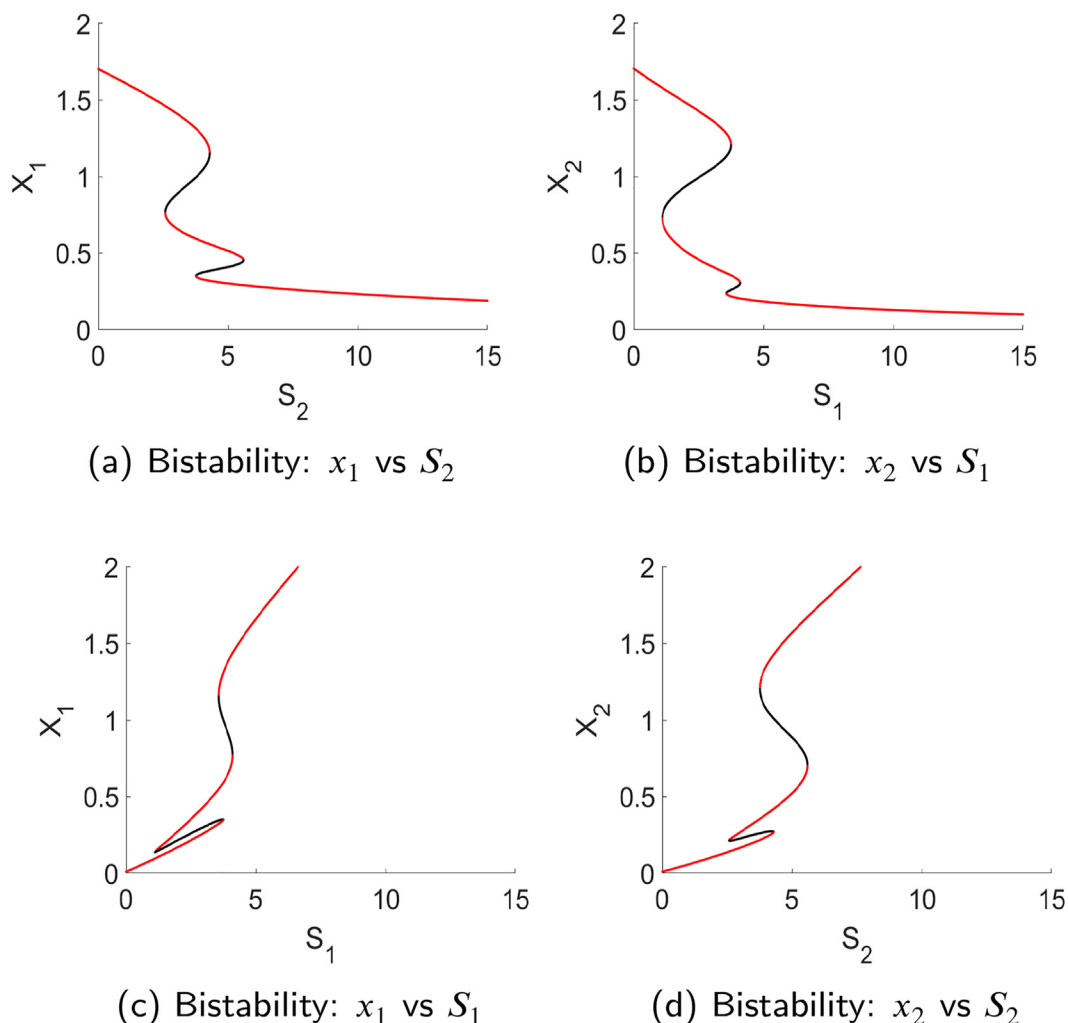


**Fig. 8.** The bifurcation diagrams for varying input signals ( $S_1$  and  $S_2$ ) against the state variables  $x_1$  and  $x_2$  show bistable dynamics (with the set  $\Theta_0$ ).

In terms of the pathways, this indicates that deactivation rates of both STAT1 and STAT6 ( $q_1$  and  $q_2$ , respectively) are highly sensitive, as well as the input signal for M1 polarization,  $INF\gamma$  ( $S_1$ ). Parameters  $k_2$  and  $k_1$  are also sensitive, and both relate to the response of the Hill functions for self-stimulation. These parameters govern the concentration at which the switch takes place. In all cases,  $k_2$  is more sensitive than  $k_1$ . Parameters  $S_2$  and  $a_2$  are the signaling input for M2 polarization (IL-4) and the maximum rate at which STAT6 stimulates its own activation via a regulative feedback mechanism.

#### 4.3. Effect of perturbation in deactivation rates $q_1$ and $q_2$

Fig. 7 illustrates that by perturbing  $q_2$  the response of transcription factors to input signals changes. The change in response seems to occur with respect to the strength of the input signal, as well as according to stability. For example, in Fig. 7(b)–(c), lower  $q_2$  values seem to increase the number of stable states, and to increase the external stimuli needed to evoke a fate change. This example indicates that deactivation rates can contribute to the robustness of the dynamical system to variations in external stimuli. In particular, it illustrates that deactivation of STAT1 and STAT6 plays an essential role in macrophage polarization, as deactivation rates indirectly

affect inhibition of external input signals on the opposite state variable, while self-stimulation affects its own state variable.

For all three parameter sets ( $\Theta_{0,1,2}$ ), an increase in the deactivation rate for STAT1,  $q_1$ , leads to a reduction in the number of steady states. For example, in the quadstable case, the system shows first tristability, then bistability, and finally monostability upon an increase of  $q_1$ , whereby first the high/high, then the low/high, and finally the low/low steady state disappear. Consequently, a system with faster STAT1 deactivation rate tends to polarize more strongly towards the M2 phenotype.

### 5. Discussion

In this work, we develop and explore a novel mathematical model for the dynamics of macrophage polarization and identify key parameters of the multi-stable dynamics. We validate that macrophage polarization is not strictly bipolar, but can consist of multiple phenotypes. Ours is the first 2-dimensional macrophage polarization model to show bistable, tristable and quadstable phenotypes. The insight gained from our model is that asymmetry in the model equations together with high non-linearity can result in high multi-stability. This is an important advance as we could validate previous biological findings on macrophage phenotypes, which so far have only been demonstrated by more detailed, com-

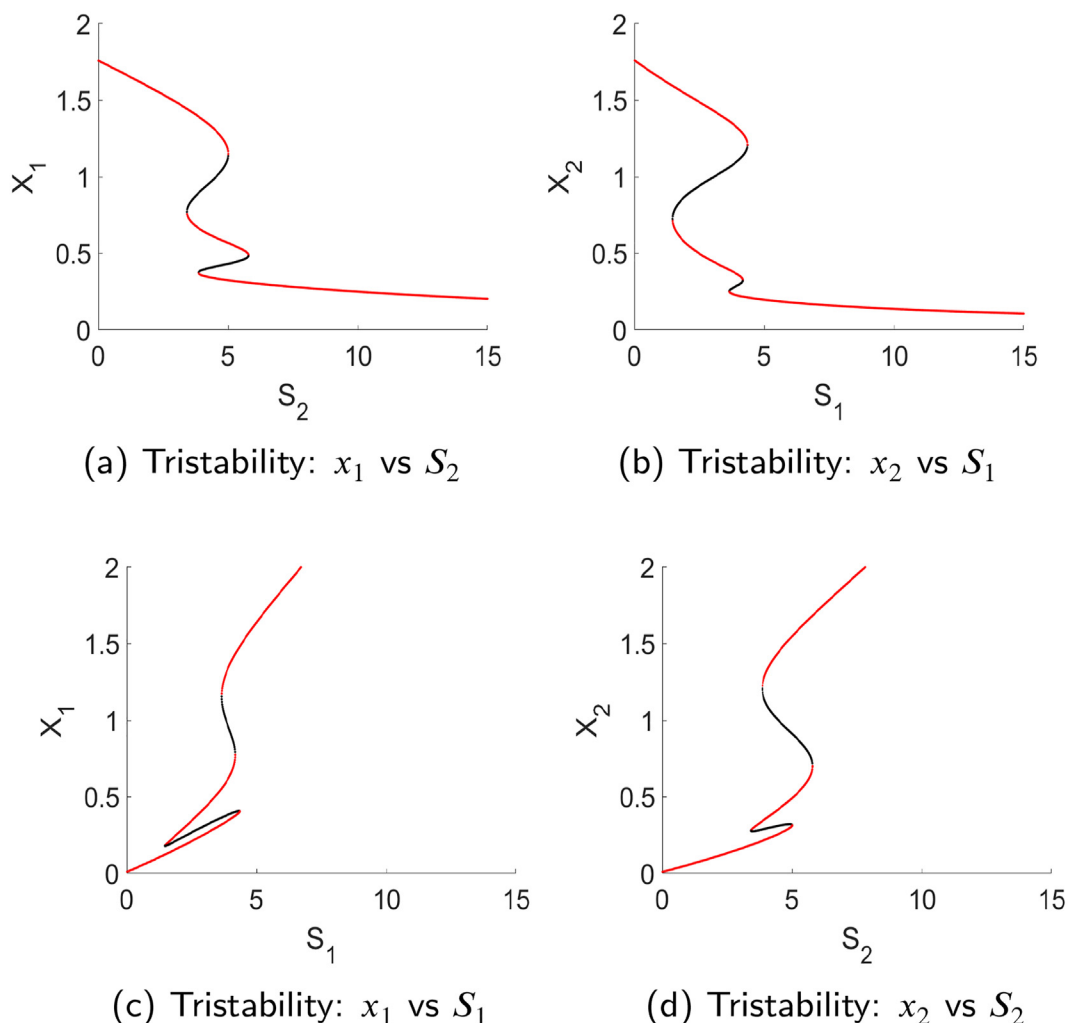


**Fig. 9.** The bifurcation diagrams for varying input signals ( $S_1$  and  $S_2$ ) against the state variables  $x_1$  and  $x_2$  show tristable dynamics (with the set  $\Theta_1$ ).

plex and multidimensional (dimensions > 2) macrophage models e.g., Zhao et al. (2019), Nickaeen et al. (2019).

We could validate known phenotypes (i.e., M0, M1 and M2) and have uncovered an unknown, intermittent one (i.e., high/high) with a mixed phenotype expression (Orekhov et al., 2019). From a biological perspective, the intermittent phenotype might more likely be observed in in vivo settings than the extreme M1 and M2 cases, which are studied in cell cultures. According to Andrecut et al. (2011), the low/low state is a “metastable state of indeterminacy”, which can switch to either M1 or M2 dependent on the input signals. This state is characterized by the fact that both STATs are at low expression level and is, according to Andrecut et al. (2011), characteristic for multipotent cells. Besides Andrecut et al. (2011), such an undetermined state has been previously described in Nickaeen et al. (2019) for macrophages and in Yates et al. (2004) for T-cells. Given the characteristics of the low-low state, it is represented in a biological context by non-activated macrophages (Orekhov et al., 2019). Although, we cannot rule out that there exist more than four different phenotypes for our system, our findings are supported by those in Lu et al. (2013), where the authors identified a maximum of four stable states given a similar model formulation. To our knowledge, only one previous study by Nickaeen et al. (2019), which studied a more complex model and applied also two- and three-dimensional bifurcation analyses, could identify a broader spectrum of known (e.g., M2a and M2b) and unknown macrophage phenotypes. Our identi-

fied unknown phenotype can however not be compared directly to those in Nickaeen et al. (2019), because the authors classified STAT activation into high, medium and low levels, while we only made a distinction between high and low. In addition, such classification states are model dependent.

Both our work and Yates’ paper (Yates et al., 2004) are examples of immune cell polarization modeled through the STAT pathways (in our case, macrophages, in Yates’ case, helper T cells). The STAT pathway is a paradigm for membrane to nucleus signaling and has come to explain how a broad range of soluble factors, including cytokines, mediate cells’ diverse functions, including polarization (Seif et al., 2017; Leonard, 2001; Villarino et al., 2017). Our model formulation is specific to what we know and understand about macrophage polarization in terms of specifically considering the signals IL-4 and IFN $\gamma$ , but general STAT pathway modeling could be applicable to a wide variety of immune cells. By comparing models for different cell types (in which the models are parameterized with biologically justified values), a sensitivity analysis could reveal which parameters are most important for specific cell types.

Sensitivity analysis of our model revealed the high impact of the deactivation rates,  $q_2$  and  $q_1$ , on the ratio of STAT1 to STAT6 activation at steady state, used as a proxy for M1 and M2 phenotype, respectively. Parameters  $k_2$  and  $a_2$  were also identified as sensitive because both of these parameters are related to the self-stimulation of STAT6 activation.

Our most sensitive model parameters are similar to those identified in Torres et al. (2019). The most sensitive parameters in our model ( $k_1, k_2, a_2, q_1, q_2$ ) and in the models by Torres et al. (2019) are parameters of activation and deactivation. The agreement in the sensitive parameters of our model with the previous models can therefore be considered a validation of the sensitivity analysis results.

These sensitive parameters agree with results of our bifurcation analysis, where parameters of self-stimulation and deactivation seemed to have a profound impact on the dynamics. For example, in the quadstable case, parameters of self-stimulation might explain the observed system commitment and the emergence of an additional phenotype, while results of varying deactivation rates changed the response to external signaling cues, as can be seen in Fig. 7. It should be noted that the observed commitment to a phenotype is not specific to this macrophage model, but rather a generic property of a toggle switch circuit model type, of which the macrophage model is a variant. However, our results are unique in the sense that they identify the parameters that drive phenotype commitment, and thus might help in replicating macrophage phenotype commitment in, e.g., laboratory experiments. The consistency in identifying sensitive parameters from bifurcation and sensitivity analyses is however expected, because a properly designed analysis should reveal bifurcation parameters to be sensitive (Marino et al. (2008)).

In summary, bifurcation and sensitivity analyses showed that external signaling cues are necessary for macrophage commitment and emergence to a phenotype, but that the intrinsic macrophage pathway (represented by self-stimulative factors and deactivation) are equally important (Geeraerts et al., 2017; Biswas and Mantovani, 2012). It should be noted that the intrinsic pathways, which enabled fate commitment in the quadstable situation, are masked by the generic nature (i.e., Hill function) of our model. Intrinsic pathways in macrophages are in general variable (Geeraerts et al., 2017).

Our results support the expectation from the model diagram (Fig. 1) that the system's outcome also depends crucially on the self-stimulation of  $x_2$ . Because the equations are not symmetric (i.e., in the second equation the stimulatory and inhibitory Hill functions are additive, not multiplicative as in the first equation), the parameters associated with STAT6 have a stronger impact on the model outcome. This observation is also reflected in the asymmetric values of  $a_1, n_1$  and  $a_2, n_2$  in  $\Theta_2$ . The asymmetry illustrates that lower values of  $a_2, n_2$  have the same effect on systems dynamics as higher values of  $a_1, n_1$ . The parameters in  $\Theta_{0,1}$  however are symmetric, because they were adapted from the mathematical model in Yates et al. (2004), which has a symmetric model structure. The need for an asymmetry in self-stimulation dynamics of STAT1 and STAT6 might be explained by the experimental finding that the signaling pathway induced by IFN- $\gamma$  dominates over the signaling pathway induced by IL-4, according to the authors in Piccolo et al. (2017). This explanation is furthermore in accordance with our finding of an irreversible switch to the M1 phenotype for high concentrations of INF- $\gamma$ .

Although our model was build based on the inhibition of STATs activation via the SOCS inhibitors, we could also connect our results to the effect of another STAT1 inhibitor, namely, the SUMO conjugation (Droescher et al., 2011; Begitt et al., 2011), thanks to the general model formulation. SUMO conjugation leads to the biochemical difference in STAT1 de-/phosphorylation dynamics compared to STAT6 (Droescher et al., 2011). We investigated its effect by analyzing faster STAT1 deactivation rates, which seem to drive the model dynamics towards the M2 phenotype.

Furthermore, we illustrated how STAT deactivation impacts macrophage polarization by influencing the robustness to external

stimuli. The authors in Sridharan et al. (2015) pointed out that the effects of deactivation are, however, not well understood for macrophages. Therefore, future experiments could aim at inhibiting kinase or phosphatase activity, in order to quantify the (de-) phosphorylation rates with time (Gelens and Saurin, 2018). For example, applying the small molecule inhibitor for SUMOylation, that was recently developed by Lv et al. (2018), could yield good parameter estimates and thereby shed further insight through additional experiments. Finally the knowledge of sensitive parameters for macrophage polarization might guide the conduction of future laboratory experiments and thus deepen our understanding of macrophage polarization.

Recent work (O'Neill et al., 2016; Galván-Peña and O'Neill, 2014; Kelly et al., 2015) indicates a resurgence of interest in immunometabolism and has revealed that through polarization, macrophages undergo a specific metabolic remodeling. M1-like inflammatory macrophages are known to employ a rapid activation of aerobic glycolysis to generate ATP (Ryan and O'Neill, 2020). Inhibition of aerobic glycolysis in macrophages blocks the M1-like phenotype even in the presence of IFN $\gamma$  (Wang et al., 2018). Aerobic glycolysis is of particular importance in the STAT1 gene transcription pathway in IFN- $\gamma$  stimulated macrophages (Mills et al., 2016) due to its production of ATP from glycolytic throughput (Wang et al., 2018). Although glycolysis is not as efficient at generating ATP as its alternative pathway (oxidative phosphorylation), it can be upregulated many-fold and therefore results in a faster production of ATP compared with oxidative phosphorylation (Phan et al., 2017).

In sum, we suggest the following hypotheses, which resulted from our analyses, to be tested experimentally:

- H1: The response-time and sensitivity of STATs to cytokine signaling levels can be altered by changing deactivation rates.
- H2: Once macrophages are committed to a phenotype, further stimulation via cytokines leaves them unchanged.
- H3: Intrinsic pathway characteristics, which correspond to aspects of self-stimulation and deactivation, determine the range and variability of observable macrophage phenotypes.
- H4: There exist intermittent phenotypes with equal STAT activation levels (i.e., defined by STAT phosphorylation levels) in laboratory experiments settings.

These hypotheses generate the following suggestions for biological experiments: (1) One could begin with IL-4 polarized macrophages (M2 phenotype) and IFN $\gamma$  stimulated macrophages (M1 phenotype), and then stimulate each with the opposite cytokine, examining subsequent levels of STAT1/6 phosphorylation in addition to the gene expression of classic STAT6 target genes as well as IFN-stimulated genes (ISGs). This experiment could reveal how dominant one stimuli is compared to the other in terms of repolarizing cells. Of course, this experiment depends on the concentration of the cytokines, but this can be normalized if one selects concentrations that induce equivalent levels of phosphorylation, nuclear localization and DNA binding. (2) An additional experiment might involve polarizing naïve macrophages with mixed concentrations of IL-4 and IFN $\gamma$  and collecting the time series data for STAT activation and gene expression of target genes to determine which stimuli is more dominant.

### 5.1. Model limitations and future work

A clear advantage of our model is its simplicity and its ability to exhibit complex dynamics in terms of multistability. One limitation due to the simplicity is that spatial distributions or different

time-scale factors of each variable could not be incorporated. In addition, our model describes only two species as proxies for the two macrophage activation states as well as two input signals whereas in reality there might be more important species and input signals, which need to be considered especially for investigating macrophage polarization on the population level.

One example is NF-κB, a protein complex which interacts with type 1 interferons, among other signals (Dorrington and Fraser, 2019). Future work could inspect a more refined signaling network, based on our model formulation. (De-)phosphorylation reactions are rapid in comparison to transcriptional gene activation (Gelens and Saurin, 2018). It is therefore relevant for future work to analyze macrophage polarization in terms of slow-fast dynamics, as well as to investigate how the effect of rapid on/off dynamics could distinguish decisions in macrophage activation from the action of similar developmental circuit models. In addition, given the difference between STAT1 versus STAT6 (de-)phosphorylation reactions, it could be relevant to experimentally estimate dephosphorylation rates ( $q_i$ ) for STAT1 and STAT6.

Another limitation of this work is that our model considers a single macrophage whereas in reality there are entire populations of macrophages which influence each other. However, understanding how a single macrophage reacts to its microenvironment is a first step to understanding population level behavior.

Mathematical models are needed to address macrophage polarization on population level and to consider input signals beyond IFN-γ and IL-4, while incorporating knowledge of dynamics of a single macrophage.

The primary focus of this manuscript has been to understand the qualitative characteristics of the proposed model. Hence extending the analysis to include empirical data is beyond this scope.

Our model represents also a solid first step towards analyzing stochastic gene expression in macrophages. In future work, we will make use of the chemical master equation and analyze how switching probabilities between different phenotypes change with variations in extrinsic and intrinsic noise levels.

### Funding sources

The research of SR was funded by Trond Mohn Foundation, Grant No. BFS2017TMT01.

### Data statement

This manuscript uses no biological or experimental data. All figures can be reproduced using the mathematical model, the parameters and numerical specifications presented in this manuscript. The code is available on github: <https://github.com/Larripa/Macrophage-Polarization-Model>.

**Table 3**  
 Numeric values for drawing bifurcation diagrams in XPPAUT. The column labels represent settings for numerical parameters in AUTO<sup>1</sup>.

Stability	Ntst	Nmax	Npr	Ds	DS <sub>min</sub>	DS <sub>max</sub>	Par <sub>min</sub>	Par <sub>max</sub>
Bi	150	2500	100	0.0001	0.0001	0.01	0	100
Tri	150	500	100	0.001	0.0001	0.02	0	100
Quad <sub>s<sub>1</sub></sub>	15	30000	100	0.0001	0.0001	0.003	-100	200
Quad <sub>s<sub>2</sub></sub>	150	20000	100	0.0001	0.0001	0.0025	0	200

<sup>1</sup>Details can also be found at <http://www.math.pitt.edu/bard/bardware/tut/xppauto.html>.

Abbreviations: Ntst, number of mesh intervals for discretization of periodic orbits, Nmax, maximum number of steps taken along any branch, Npr, give complete info every Npr steps, Ds, initial step size for bifurcation calculation, DS<sub>min</sub>, minimum step size, DS<sub>max</sub>, maximum step size, Par<sub>min</sub>, left-hand limit of the diagram for principal parameter, Par<sub>max</sub>, right-hand limit of the diagram for the principal parameter.

### Declaration of Competing Interest

The authors declare that they have no known competing financial interests or personal relationships that could have appeared to influence the work reported in this paper.

### CRediT authorship contribution statement

**Anna S Frank:** Methodology, Software, Validation, Formal analysis, Investigation, Writing - original draft, Writing - review & editing, Visualization. **Kamila Larripa:** Conceptualization, Methodology, Software, Validation, Formal analysis, Investigation, Writing - original draft, Writing - review & editing, Visualization, Funding acquisition. **Hwayeon Ryu:** Conceptualization, Methodology, Software, Validation, Formal analysis, Investigation, Writing - original draft, Writing - review & editing, Visualization, Funding acquisition. **Ryan G Snodgrass:** Validation, Investigation, Writing - review & editing. **Susanna Röblitz:** Conceptualization, Methodology, Software, Validation, Formal analysis, Investigation, Writing - review & editing, Supervision, Funding acquisition.

### Acknowledgments

The authors thank the American Institute of Mathematics for providing support through its Structured Quartet Research Ensembles program.

### Appendix A. Appendix

#### A.1. Numerical details for bifurcation diagrams

Table 3 shows the numerical details used to calculate the bifurcation diagrams.

#### A.2. Sobol's method

Model output  $f(x)$  is decomposed into the sums of variances (Sobol, 2001):

$$f(x) = f_0 + \sum_{i=1}^k f_i(x_i) + \sum_{i=1}^k \sum_{j=i+1}^k f_{ij}(x_i, x_j) + \dots + f_{1\dots k}(x_1, x_2, \dots, x_k). \tag{5}$$

Here,  $f_i$  is the effect of varying  $x_i$  alone (first-order sensitivity), and  $f_{ij}$  is the effect of varying  $x_i$  and  $x_j$  simultaneously, additional to the effect of their individual variations, termed a second-order sensitivity. Higher order terms have analogous interpretations.

Assuming that  $f(x)$  is square integrable, the functional decomposition may be squared and integrated and the total variance D can be defined as

$$D = \int f^2(x) - (f_0)^2 dx \quad (6)$$

The partial variances from squaring and integrating the right hand side of Eq. (5) are of the form

$$D_{i_1, i_2, \dots, i_k} = \int \dots \int f^2(x_{i_1}, x_{i_2}, \dots, x_{i_s}) dx_{i_1} dx_{i_2} \dots dx_{i_s} \quad (7)$$

These integrals can then be approximated with Monte Carlo integration, and the Sobol sensitivity indices are calculated by the ratio of partial to total variance, representing the fraction of total variance which is attributed to individual model parameters or to combinations of parameters.

$$S_{i_1, i_2, \dots, i_s} = \frac{D_{i_1, i_2, \dots, i_s}}{D} \quad (8)$$

Furthermore, the total effect sensitivity index was proffered as an extension of the Sobol sensitivity index to quantify the overall effect of a parameter alone and in combination with any other parameters on model output (Homma and Saltelli, 1996). This is defined to be

$$S_{T_i} = S_i + S_{c_i} \quad (9)$$

where  $S_{c_i}$  is the set of sensitivity indices in which parameter  $x_i$  appears.

### A.3. Bifurcation diagrams for the bistable and tristable case

Figs. 8 and 9 show the bifurcation diagrams for the bistable and tristable case.

## References

Andrecut, M., Halley, J.D., Winkler, D.A., Huang, S., 2011. A general model for binary cell fate decision gene circuits with degeneracy: indeterminacy and switch behavior in the absence of cooperativity. *PLoS One* 6. <https://doi.org/10.1371/journal.pone.0019358> e193518.

Begitt, A., Droscher, M., Knobloch, K.P., Vinkemeier, U., 2011. Sumo conjugation of STAT1 protects cells from hyperresponsiveness to IFN $\gamma$ . *Blood* 118, 1002–1007. <https://doi.org/10.1182/blood-2011-04-347930>.

Biswas, S.K., Mantovani, A., 2010. Macrophage plasticity and interaction with lymphocyte subsets: cancer as a paradigm. *Nat. Immunol.* 11, 889–896. <https://doi.org/10.1038/ni.1937>.

Biswas, S.K., Mantovani, A., 2012. Orchestration of metabolism by macrophages. *Cell Metab.* 15, 432–437. <https://doi.org/10.1016/j.cmet.2011.11.013>.

Bronte, V., Murray, P.J., 2015. Understanding local macrophage phenotypes in disease: modulating macrophage function to treat cancer. *Nat. Med.* 21, 117–119. <https://doi.org/10.1038/nm.3794>.

Brown, J.M., Recht, L., Strober, S., 2017. The promise of targeting macrophages in cancer therapy. *Clin. Cancer Res.* 23, 3241–3250. <https://doi.org/10.1158/1078-0432.CCR-16-3122>.

Callard, R.E., 2007. Decision-making by the immune response. *Immunol. Cell Biol.* 85, 300–305.

Castiglione, F., Tieri, P., Palma, A., Jarrah, A.S., 2016. Statistical ensemble of gene regulatory networks of macrophage differentiation. *BMC Bioinf.* 17, 506. <https://doi.org/10.1186/s12859-016-1363-4>.

Cheng, H., Wang, Z., Fu, L., Xu, T., 2019. Macrophage polarization in the development and progression of ovarian cancers: an overview. *Front. Oncol.* 9, 421. <https://doi.org/10.3389/fonc.2019.00421>.

Das, A., Sinha, M., Datta, S., Abas, M., Chaffee, S., Sen, C.K., Roy, S., 2015. Monocyte and macrophage plasticity in tissue repair and regeneration. *Am. J. Pathol.* 185, 2596–2606. <https://doi.org/10.1016/j.ajpath.2015.06.001>.

Dempoya, J., Matsumiya, T., Imaizumi, T., Hayakari, R., Xing, F., Yoshida, H., Okumura, K., Satoh, K., 2012. Double-stranded RNA induces biphasic STAT1 phosphorylation by both type I interferon (IFN)-dependent and type I IFN-independent pathways. *J. Virol.* 86, 12760–12769. <https://doi.org/10.1128/JVI.01881-12>.

Dickensheets, H.L., Venkataraman, C., Schindler, U., Donnelly, R.P., 1999. Interferons inhibit activation of STAT6 by interleukin 4 in human monocytes by inducing SOCS-1 gene expression. *Proc. Natl. Acad. Sci. USA* 96, 10800–10805. <https://doi.org/10.1073/pnas.96.19.10800>.

Dorrington, M.G., Fraser, I.D., 2019. NF- $\kappa$ B signaling in macrophages: dynamics, cross-talk, and signal integration. *Front. Immunol.* 10, 705. <https://doi.org/10.3389/fimmu.2019.00705>.

Droscher, M., Begitt, A., Marg, A., Zacharias, M., Vinkemeier, U., 2011. Cytokine-induced paracrystals prolong the activity of STAT transcription factors and provide a model for the regulation of protein-solubility by SUMO. *J. Biol. Chem.* 286, 18731–18746. <https://doi.org/10.1074/jbc.M111.235978>.

Ermentrout, B., 2001. XPPAUT 5.0—the differential equations tool. <http://www.math.pitt.edu/bard/xpp/xpp.html> (accessed November, 2019).

Fraternal, A., Brundu, S., Magnani, M., 2015. Polarization and repolarization of macrophages. *J. Clin. Cell. Immunol.* 6, 2. <https://doi.org/10.4172/2155-9899.1000319>.

Galván-Peña, S., O'Neill, L.A., 2014. Metabolic reprogramming in macrophage polarization. *Front. Immunol.* 5, 420.

Gardner, T.S., Cantor, C.R., Collins, J.J., 2000. Construction of a genetic toggle switch in *Escherichia coli*. *Nature* 403, 339–342.

Geeraerts, X., Bolli, E., Fendt, S.M., Van Ginderachter, J.A., 2017. Macrophage metabolism as therapeutic target for cancer, atherosclerosis, and obesity. *Front. Immunol.* 8, 289. <https://doi.org/10.3389/fimmu.2017.00289>.

Gelens, L., Saurin, A.T., 2018. Exploring the function of dynamic phosphorylation-dephosphorylation cycles. *Dev. Cell* 44, 659–663. <https://doi.org/10.1016/j.devcel.2018.03.002>.

Goenka, S., Kaplan, M.H., 2011. Transcriptional regulation by STAT6. *Immunol. Res.* 50, 87–96. <https://doi.org/10.1007/s12026-011-8205-2>.

Gordon, S., 2003. Alternative activation of macrophages. *Nat. Rev. Immunol.* 3, 23–35. <https://doi.org/10.1038/nri978>.

Gul, R., Bernhard, S., 2018. Sensitivity analysis: a useful tool for bifurcation analysis. In: Lopez-Ruiz, R. (Ed.), *Complexity in Biological and Physical Systems: Bifurcations, Solitons and Fractals*. Intech Open Limited, London, UK, p. 69. <https://doi.org/10.5772/intechopen.72345>. Chapter 4.

Herman, J., Usher, W., 2017. SALib: an open-source python library for sensitivity analysis. *J. Open Source Softw.* 2. 10.21105/joss.00097.

ten Hoeve, J., de Jesus Ibarra-Sanchez, M., Fu, Y., Zhu, W., Tremblay, M., David, M., Shuai, K., 2002. Identification of a nuclear STAT1 protein tyrosine phosphatase. *Mol. Cell Biol.* 22, 5662–5668. <https://doi.org/10.1128/mcb.22.16.5662-5668.2002>.

Homma, T., Saltelli, A., 1996. Importance measures in global sensitivity analysis of nonlinear models. *Reliab. Eng. Syst. Saf.* 52, 1–17. [https://doi.org/10.1016/0951-8320\(96\)00002-6](https://doi.org/10.1016/0951-8320(96)00002-6).

Kelly, B., O'Neill, L.A., 2015. Metabolic reprogramming in macrophages and dendritic cells in innate immunity. *Cell Res.* 25, 771–784.

Kovarik, P., Stoiber, D., Eysers, P.A., Menghini, R., Neiningner, A., Gaestel, M., Cohen, P., Decker, T., 1999. Stress-induced phosphorylation of STAT1 at Ser727 requires p38 mitogen-activated protein kinase whereas IFN- $\gamma$  uses a different signaling pathway. *Proc. Nat. Acad. Sci.* 96, 13956–13961.

Kuang, D.M., Zhao, Q., Peng, C., Xu, J., Zhang, J.P., Wu, C., Zheng, L., 2009. Activated monocytes in peritumoral stroma of hepatocellular carcinoma foster immune privilege and disease progression through pd-1. *J. Exp. Med.* 206, 1327–1337. <https://doi.org/10.1084/jem.20082173>.

Lawrence, T., Natoli, G., 2011. Transcriptional regulation of macrophage polarization: enabling diversity with identity. *Nat. Rev. Immunol.* 11, 750–761. <https://doi.org/10.1038/nri3088>.

Lee, K.Y., 2019. M1 and M2 polarization of macrophages: a mini-review. *Med. Biol. Sci. Eng.* 2, 1–5. <https://doi.org/10.30579/mbse.2019.2.1.1>.

Leonard, W.J., 2001. Role of JAK kinases and STATs in cytokine signal transduction. *Int. J. Hematol.* 73, 271–277.

Lin, E.Y., Nguyen, A.V., Russell, R.G., Pollard, J.W., 2001. Colony-stimulating factor 1 promotes progression of mammary tumors to malignancy. *J. Exp. Med.* 193, 727–740. <https://doi.org/10.1084/jem.193.6.727>.

Linde, N., Gutschalk, C.M., Hoffmann, C., Yilmaz, D., Mueller, M.M., 2012. Integrating macrophages into organotypic co-cultures: a 3d in vitro model to study tumor-associated macrophages. *PLoS One* 7, <https://doi.org/10.1371/journal.pone.0040058> e40058.

Lu, M., Jolly, M.K., Gomoto, R., Huang, B., Onuchic, J., Ben-Jacob, E., 2013. Tristability in cancer-associated microRNA-TF chimera toggle switch. *J. Phys. Chem. B* 117, 13164–13174. <https://doi.org/10.1021/jp403156m>.

Luckheeram, R.V., Zhou, R., Verma, A.D., Xia, B., 2012. Cd4+ T cells: differentiation and functions. *Clin. Dev. Immunol.* 2012, <https://doi.org/10.1155/2012/925135> 925135.

Lv, Z., Yuan, L., Atkinson, J.H., Williams, K.M., Vega, R., Sessions, E.H., Divlianska, D.B., Davies, C., Chen, Y., Olsen, S.K., 2018. Molecular mechanism of a covalent allosteric inhibitor of SUMO E1 activating enzyme. *Nat. Commun.* 9, 5145. <https://doi.org/10.1038/s41467-018-07015-1>.

Marino, S., Hogue, I.B., Ray, C.J., Kirschner, D.E., 2008. A methodology for performing global uncertainty and sensitivity analysis in systems biology. *J. Theor. Biol.* 254, 178–196. <https://doi.org/10.1016/j.jtbi.2008.04.011>.

Martinez, F.O., Gordon, S., 2014. The M1 and M2 paradigm of macrophage activation: time for reassessment. *F1000Prime Rep.* 6, 10.12703/P6-13.

Medzhitov, R., 2008. Origin and physiological roles of inflammation. *Nature* 454, 428–435. <https://doi.org/10.1038/nature07201>.

Mills, E.L., Kelly, B., Logan, A., Costa, A.S., Varma, M., Bryant, C.E., Tourlomousis, P., Däbritz, J.H.M., Gottlieb, E., Latorre, I., et al., 2016. Succinate dehydrogenase supports metabolic repurposing of mitochondria to drive inflammatory macrophages. *Cell* 167, 457–470.

Morales, V., Soto-Ortiz, L., 2018. Modeling macrophage polarization and its effect on cancer treatment success. *Open J. Immunol.* 8, 36.

Mosser, D.M., Edwards, J.P., 2008. Exploring the full spectrum of macrophage activation. *Nat. Rev. Immunol.* 8, 958–969. <https://doi.org/10.1038/nri2448>.

- Namgaladze, D., Snodgrass, R.G., Angioni, C., Grossmann, N., Dehne, N., Geisslinger, G., Brüne, B., 2015. AMP-activated protein kinase suppresses arachidonate 15-lipoxygenase expression in interleukin 4-polarized human macrophages. *J. Biol. Chem.* 290, 24484–24494.
- Nickaen, N., Ghaisari, J., Heiner, M., Moein, S., Gheisari, Y., 2019. Agent-based modeling and bifurcation analysis reveal mechanisms of macrophage polarization and phenotype pattern distribution. *Sci. Rep.* 9, 12764. <https://doi.org/10.1038/s41598-019-48865-z>.
- Ohmori, Y., Hamilton, T.A., 1997. IL-4-induced STAT6 suppresses IFN- $\gamma$ -stimulated STAT1-dependent transcription in mouse macrophages. *J. Immunol.* 159, 5474–5482.
- O'Neill, L.A., Kishton, R.J., Rathmell, J., 2016. A guide to immunometabolism for immunologists. *Nat. Rev. Immunol.* 16, 553.
- Orekhov, A.N., Orekhova, V.A., Nikiforov, N.G., Myasoedova, V.A., Grechko, A.V., Romanenko, E.B., Zhang, D., Chistiakov, D.A., 2019. Monocyte differentiation and macrophage polarization. *Vessel Plus* 3. [10.20517/2574-1209.2019.04](https://doi.org/10.20517/2574-1209.2019.04).
- Palma, A., Jarrah, A.S., Tieri, P., Cesareni, G., Castiglione, F., 2018. Gene regulatory network modeling of macrophage differentiation corroborates the continuum hypothesis of polarization states. *Front. Physiol.* 9, 1659. <https://doi.org/10.3389/fphys.2018.01659>.
- Phan, A.T., Goldrath, A.W., Glass, C.K., 2017. Metabolic and epigenetic coordination of T cell and macrophage immunity. *Immunity* 46, 714–729.
- Piccolo, V., Curina, A., Genua, M., Ghisletti, S., Simonatto, M., Sabò, A., Amati, B., Ostuni, R., Natoli, G., 2017. Opposing macrophage polarization programs show extensive epigenomic and transcriptional cross-talk. *Nat. Immunol.* 18, 530–540. <https://doi.org/10.1038/ni.3710>.
- Ryan, D.G., O'Neill, L.A., 2020. Krebs cycle reborn in macrophage immunometabolism. *Annu. Rev. Immunol.* 38, 289–313.
- Saccani, A., Schioppa, T., Porta, C., Biswas, S.K., Nebuloni, M., Vago, L., Bottazzi, B., Colombo, M.P., Mantovani, A., Sica, A., 2006. p50 nuclear factor- $\kappa$ B overexpression in tumor-associated macrophages inhibits M1 inflammatory responses and antitumor resistance. *Cancer Res.* 66, 11432–11440. <https://doi.org/10.1158/0008-5472.CAN-06-1867>.
- Seif, F., Khoshmirasfa, M., Aazami, H., Mohsenzadegan, M., Sedighi, G., Bahar, M., 2017. The role of JAK-STAT signaling pathway and its regulators in the fate of T helper cells. *Cell Commun. Signal.* 15, 1–13.
- Sica, A., Invernizzi, P., Mantovani, A., 2014. Macrophage plasticity and polarization in liver homeostasis and pathology. *Hepatology* 59, 2034–2042. <https://doi.org/10.1002/hep.26754>.
- Smith, T.D., Tse, M.J., Read, E.L., Liu, W.F., 2016. Regulation of macrophage polarization and plasticity by complex activation signals. *Integr. Biol. (Camb.)* 8, 946–955. <https://doi.org/10.1039/c6ib00105j>.
- Sobol, I.M., 2001. Global sensitivity indices for nonlinear mathematical models and their Monte Carlo estimates. *Math. Comput. Simulat.* 55, 271–280. [https://doi.org/10.1016/S0378-4754\(00\)00270-6](https://doi.org/10.1016/S0378-4754(00)00270-6).
- Sridharan, R., Cameron, A.R., Kelly, D.J., Kearney, C.J., O'Brien, F.J., 2015. Biomaterial based modulation of macrophage polarization: a review and suggested design principles. *Mater. Today* 18, 313–325. <https://doi.org/10.1016/j.mattod.2015.01.019>.
- Torres, M., Wang, J., Yannie, P.J., Ghosh, S., Segal, R.A., Reynolds, A.M., 2019. Identifying important parameters in the inflammatory process with a mathematical model of immune cell influx and macrophage polarization. *PLoS Comput. Biol.* 15. <https://doi.org/10.1371/journal.pcbi.1007172> e1007172.
- Tyson, J.J., Novák, B., 2010. Functional motifs in biochemical reaction networks. *Ann. Rev. Phys. Chem.* 61, 219–240. <https://doi.org/10.1146/annurev.physchem.012809.103457>.
- Umemura, N., Saio, M., Suwa, T., Kitoh, Y., Bai, J., Nonaka, K., Ouyang, G.F., Okada, M., Balazs, M., Adany, R., et al., 2008. Tumor-infiltrating myeloid-derived suppressor cells are pleiotropic-inflamed monocytes/macrophages that bear M1-and M2-type characteristics. *J. Leukoc. Biol.* 83, 1136–1144. <https://doi.org/10.1189/jlb.0907611>.
- Venkataraman, C., Leung, S., Salvekar, A., Mano, H., Schindler, U., 1999. Repression of IL-4-induced gene expression by IFN- $\gamma$  requires STAT1 activation. *J. Immunol.* 162, 4053–4061.
- Villarino, A.V., Kanno, Y., O'Shea, J.J., 2017. Mechanisms and consequences of JAK-STAT signaling in the immune system. *Nat. Immunol.* 18, 374.
- Wang, F., Zhang, S., Jeon, R., Vuckovic, L., Jiang, X., Lerman, A., Folmes, C.D., Dzeja, P. D., Herrmann, J., 2018. Interferon gamma induces reversible metabolic reprogramming of M1 macrophages to sustain cell viability and pro-inflammatory activity. *EBioMedicine* 30, 303–316.
- Wang, N., Liang, H., Zen, K., 2014. Molecular mechanisms that influence the macrophage M1–M2 polarization balance. *Front. Immunol.* 5, 614. <https://doi.org/10.3389/fimmu.2014.00614>.
- Williams, C.B., Yeh, E.S., Soloff, A.C., 2016. Tumor-associated macrophages: unwitting accomplices in breast cancer malignancy. *NPJ Breast Cancer* 2, 15025. <https://doi.org/10.1038/nnpjbcancer.2015.25>.
- Yarilina, A., Park-Min, K.H., Antoniv, T., Hu, X., Ivashkiv, L.B., 2008. TNF activates an IRF1-dependent autocrine loop leading to sustained expression of chemokines and STAT1-dependent type I interferon-response genes. *Nat. Immunol.* 9, 378–387. <https://doi.org/10.1038/ni1576>.
- Yates, A., Callard, R., Stark, J., 2004. Combining cytokine signalling with T-bet and GATA-3 regulation in Th1 and Th2 differentiation: a model for cellular decision-making. *J. Theor. Biol.* 231, 181–196. <https://doi.org/10.1016/j.jtbi.2004.06.013>.
- Zhao, C., Miranda, A.C., Sové, R.J., Medeiros, T.X., Annex, B.H., Popel, A.S., 2019. A mechanistic integrative computational model of macrophage polarization: Implications in human pathophysiology. *PLoS Comput. Biol.* 15. <https://doi.org/10.1371/journal.pcbi.1007468> e1007468.
- Zheng, X., Turkowski, K., Mora, J., Brüne, B., Seeger, W., Weigert, A., Savai, R., 2017. Redirecting tumor-associated macrophages to become tumoricidal effectors as a novel strategy for cancer therapy. *Oncotarget* 8, 48436–48452. [10.18632/oncotarget.17061](https://doi.org/10.18632/oncotarget.17061).
- Zi, Z., 2011. Sensitivity analysis approaches applied to systems biology models. *IET Syst. Biol.* 5, 336–346. <https://doi.org/10.1049/iet-syb.2011.0015>.